

PERFORMANCE ANALYSIS OF AN EFFICIENT NEW-DESIGN SOLAR AIR HEATER BY CFD METHOD

Maryam Moein Addini and Seyyed Abdolreza Gandjalikhan Nassab*

Mechanical Engineering Department, School of Engineering, Shahid Bahonar University of Kerman, Kerman, Iran

e-mail: ma.moein@eng.uk.ac.ir, ganj110@uk.ac.ir

*corresponding author

Abstract

The main contribution of this study is to present a modified V-corrugated grooved absorber plate in the construction of plane solar air heaters for higher performance. The combined effects of extended heat transfer area due to the V-shaped absorber, the suction process by the grooves that maintains the convective flow closed to the heated absorber and the jet impingement enable high efficiency of the proposed solar collector. For simulation purposes, the conduction equation is employed for temperature computations inside the solid elements, while the turbulent airflow equations are solved based on the CFD method using the $\kappa - \varepsilon$ turbulence model. The present finite element-based analysis is performed using the COMSOL Multi-physics software. To demonstrate the rate of irreversibilities in a solar collector, the entropy generation due to heat transfer and viscous friction and, accordingly, the second law efficiency are computed at different steady operating conditions. The numerical procedure is validated by comparing the obtained numerical findings with the experimental results reported in the literature. From the obtained results, it is found that the proposed absorber plate has a triple-edged sword positive effect on the solar air heater performance, such that the thermal efficiencies up to 80% are computed. Moreover, about 10% improvement in the thermal efficiency of the proposed solar collector compared with its competitor (solar air heater with a simple V-corrugated absorber) reveals the positive impact of the designed absorber plate. Also, the increase in the height of V-shaped absorber from $H_0 = 2 \text{ cm}$ to $H_0 = 4 \text{ cm}$ leads to about 11% improvement in the heater thermal efficiency. The numerical findings can be considered as a good reference to find an alternative for efficient solar collectors.

Keywords: Solar air heater, V-shaped absorber, suction, jet impingement, CFD.

1. Introduction

Today, the availability of each form of energy becomes the leading global concern, and to meet the rising demand, plenty of available energy resources are employed. Solar energy as an inexpensive alternative energy source can be considered in the consumption of energy. Solar air heaters are collectors that convert incoming solar radiation into useful heat energy, among which are the plane solar air heaters (SAHs) that have simple structure and design with low maintenance. However, these heat exchangers do not achieve high efficiency due to low air conductivity and heat capacity, which leads to small value of convection coefficient between the convection air flow and the heated surface inside the collector. To increase the performance of SAH, researchers

seek different ways. Mohamadi (2013) examined the effect of extended surfaces, Khanlari (2021) investigated the behavior of different flow types on convection heat transfer and Afshar (2020) used vortex generators for increasing the performance of solar collectors. It is clear that the absorber plate is the most important part of SAH and many studies have been carried out on the optimization of the absorber geometry. Many researchers have suggested the performance improvement by employing ribs on the heated surface. Alam (2017) suggested the performance improvement by employing conical protrusion roughness ribs. Saravanakumar (2020) used arc shaped rib and Wang (2020) suggested "S" shaped ribs with gap for enhancing the rate of convection heat transfer. Another way for enhancing heat transfer is using baffles with different shapes, such that this technique was examined by Bayrak (2013), El-Said (2020), Fiuk (2019), Hachemi (1995), Chabane (2014) and Yang (2014). Replacing flat plate absorber with V-groove corrugated absorber is another method for performance improvement and many investigators including Ho (2017), Desisa (2020) and El-Sebaai (2011) studied about this technique. A numerical analysis of solar air dryer with a V-groove double pass collector carried out by Hassan (2022) and the obtained findings which revealed the positive effect of the applied method were validated with experiment.

In the experimental research work by Alomar (2022), a modified v-corrugated absorber plate was employed in the construction of plane SAH to get a better performance. The applied absorber was perforated for having the jet impingement and higher convection heat transfer on the heated surface. The performances of the normal and modified v-corrugated SAH with the jet plate blown systems were compared to prove the advantages of the modified solar heater. Some experiments have been done in winter season in Iraq and the obtained results showed that the modified heater has more efficiency than the base mode by 11.5 %, 14.5 %, 12.3 % and 13.2 % for air flow rates of 9 g/s, 18 kg/s, 28 g/s and 37 g/s, respectively.

In a theoretical and CFD based study by Nidhul (2020), SAHs with W-baffles and semi-cylindrical sidewalls were analyzed in the turbulent air flow regime for energy and exergy efficiencies. The effects of baffle height and baffle pitch on the thermo-hydrodynamic characteristics of solar collector were examined for a fixed inclined angle of baffles.

To examine the role of a novel discrete double arc roughness with reverse form in improving the thermal performance of solar heater, an indoor experimental work was carried out by Agrawal (2022) and 2.66 times increase in the value of convection coefficient was reported compared to a smooth channel.

In a theoretical and experimental analysis by Arya (2023), the use of V shape, arc and transverse broken-miniature in SAHs combined with dimples on an absorber was examined. As the main result, it was found that among the different geometrical shapes of miniature, the 90° transverse broken one has the best performance at Re below 10,000.

As the continuation of the previous work, an attempt was made in the present study to introduce a new and applicable technique for improving the performance of SAHs with combining the benefits of three existing methods including the use of V-corrugated absorber plate (for increasing the surface area), the suction process (for having a thin boundary layer and preventing from flow separation) and finally employing jet impingement, simultaneously. To reach this goal, the current study introduces a numerical simulation of the proposed SAH by simultaneous solution of the governing equations for the turbulent air flow, including the continuity, momentum, energy and the Laplace equation for the glass cover, absorber, bottom plate and insulation layer. In velocity, pressure and temperature computations, all numerical solutions were performed by the COMSOL Multi-Physics software. Finally, the performance of designed SAH operating under different steady conditions was examined both via energy and exergy considerations.

2. Theory

The geometry of the simulated plane SAH is depicted in Fig. 1. It includes the glass cover, air channels, absorber, bottom plate and insulation layer. A schematic of the proposed grooved V-corrugated absorber plate is drawn in Fig. 2. The first groove at the upstream side has the maximum thickness of $t_0 = 6.5 \text{ mm}$, such that for the subsequent grooves the thickness t is decreased with $\Delta t = 0.8 \text{ mm}$ for having almost the same air flow rate in all jet flows. In Table 1, the values of some geometrical parameters of the simulated SAH are reported. The airflow enters from the inlet section due to the air blower suction, and the forced convection heat transfer occurs with the heated absorber and bottom plate surfaces. Three air mass flow rates consist of $\dot{m} = 0.02 \text{ kg/s}$, 0.04 kg/s and 0.08 kg/s correspond to the range of Reynolds number ($Re = \rho b \bar{V} / \mu$) $1750 \leq Re \leq 7000$ are considered in several test cases. In numerical simulation, a great part of incoming solar heat flux, i.e. $\tau_g \times q_{sun}$, is assumed to be transmitted from the glass sheet and absorbs by the absorber plate whose black painted surface has the absorptivity of $\alpha_{abs} = 0.95$. The glass cover behaves as an opaque body against the long wave radiation emitted by the absorber and is transparent against the incoming short wave solar heat flux. The surfaces of the insulation layer and glass cover adjacent to the surrounding are in heat transfer by convection and surface radiation.

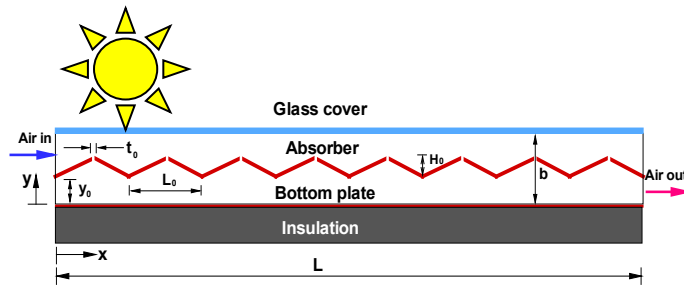


Fig. 1. A schematic of the proposed SAH.

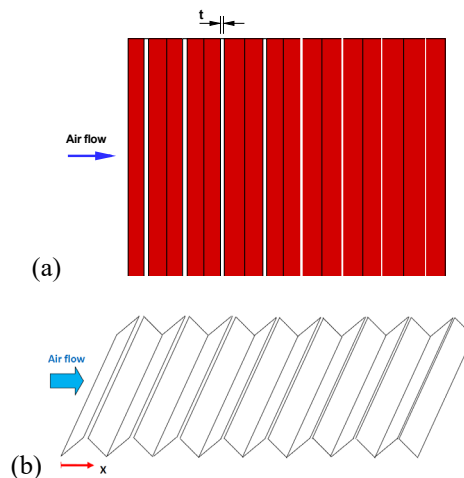


Fig. 2. The geometry of V-corrugated absorber plate. (a) The top view of absorber; (b) Three-dimensional schematic of absorber.

Parameter	Abbreviation	Value
Thickness of glass cover	δ_g	4 mm
Glass emissivity	ε_g	0.9
Glass absorptivity	α_g	0.03
Glass transmissivity	τ_g	0.95
Conduction coefficient of glass	k_g	0.78 W / mK
Conduction coefficient of insulation	k_{ins}	0.037 W / mK
Air average velocity	\bar{V}_{air}	0.8-3.2 m/s
Heater length	L	100 cm
Height of air duct	b	8 cm
Thickness of absorber	δ_{abs}	3 mm
Emissivity of absorber	ε_{abs}	0.95
Conduction coefficient of absorber	k_{abs}	400 W / mK
Inlet temperature	T_{in}	20°C
Insulation thickness	δ_{ins}	3 cm
Geometrical parameter (Fig. 1)	y_0	3 cm
Air mass flow rate	\dot{m}	0.02-0.08 kg/s
Groove thickness	t_0	6.5 mm
Thickness of bottom plate	δ_{bp}	3 mm

Table 1. Parameter values of the test cases.

2.1 Governing equations

The model is steady two-dimensional, incompressible and turbulent and the Reynolds Average Navier Stokes (RANS) equations are employed in the fluid flow computations. The k- ε model given by Patankar (1966) is used in flow computation and the enhanced wall function is considered for the grid point near the solid walls. The following flow equations written in tensor forms are considered in this study:

$$\frac{\partial u_i}{\partial x_i} = 0 \quad (1)$$

$$u_j \frac{\partial u_i}{\partial x_j} = \frac{1}{\rho} \frac{\partial p}{\partial x_i} + \frac{1}{\rho} \frac{\partial}{\partial x_j} [(\mu + \mu_t) (\frac{\partial u_i}{\partial x_j} + \frac{\partial u_j}{\partial x_i})] \quad (2)$$

$$u_j \frac{\partial T}{\partial x_j} = \frac{\partial}{\partial x_j} \left[\left(\frac{\mu}{Pr} + \frac{\mu_t}{Pr_t} \right) \frac{\partial T}{\partial x_j} \right] \quad (3)$$

In equations 1 to 3, u_i is the velocity component, T the air temperature, μ the air dynamic viscosity, ρ the air density, Pr the Prandtl number, μ_t the eddy viscosity and Pr_t is the eddy Prandtl number.

Since, the k- ϵ model is employed for computations of turbulence terms, the turbulent kinetic energy 'k' and the dissipation rate ' ϵ ' are needed, which can be obtained by the following transport equations:

$$\rho u_i \frac{\partial k}{\partial x_i} = \frac{\partial}{\partial x_j} \left[\left(\mu + \frac{\mu_t}{\sigma_k} \right) \frac{\partial k}{\partial x_j} \right] + G_k - \rho \epsilon \quad (4)$$

$$\rho u_i \frac{\partial \epsilon}{\partial x_i} = \frac{\partial}{\partial x_j} \left[\left(\mu + \frac{\mu_t}{\sigma_\epsilon} \right) \frac{\partial \epsilon}{\partial x_j} \right] + C_{\epsilon 1} \frac{\epsilon}{k} G_k - C_{\epsilon 2} \rho \frac{\epsilon^2}{k} \quad (5)$$

In these equations, the model constant values are $C_{\epsilon 1} = 1.44$, $C_{\epsilon 2} = 1.92$, $\sigma_k = 1$, and $\sigma_\epsilon = 1.3$. Also, G_k represents the turbulence kinetic energy generation due to the velocity gradient. For temperature computation in all solid elements of SAH, the Laplace equation is solved, such that the conduction equation for the glass cover contains the source term, $S_T = \alpha_g q_{sun} / \delta_g$ due to the radiative absorption by this element.

2.2 Boundary conditions

The following boundary conditions are applied in the numerical solution of governing equations:

- No slip condition in velocity computation was imposed.
- Air enters from the inlet section into the SAH with fully developed velocity profile and ambient temperature $T_{in} = 293$ K, whose kinetic energy of turbulence is $0.001 \bar{V}^2$.
- The pressure outlet was applied at the outlet section as the boundary condition.
- On the upper surface of absorber, a constant heat flux $\alpha_{abs} \times q_{sun} \times \tau_g (W/m^2)$ due to the absorbed incoming solar radiation was employed.
- At the upper surface of glass cover and lower surface of insulation, the convection boundary condition with $h_{eq} = h_{conv} + h_{rad}$, was considered.
- The radiative and convective parts of the equivalent convection coefficient are computed according to the relations reported in a paper by Duffie (2013):

$$h_{rad} = \sigma \varepsilon_g \left(\frac{T_g^4 - T_{sky}^4}{T_g - T_{amb}} \right) \quad (6)$$

$$h_{conv} = 5.7 + 3.8V_{wind} \quad (7)$$

Where the sky temperature can be calculated with the following relation:

$$T_{sky} = 0.0552 T_{amb}^{1.5} \quad (8)$$

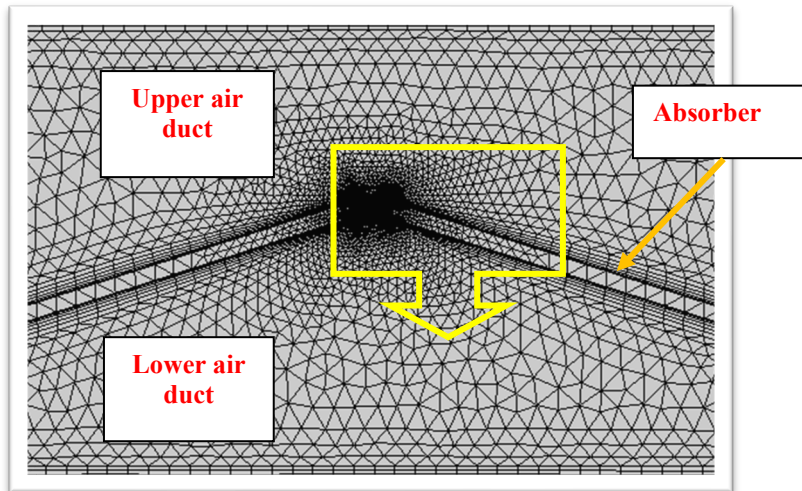
3. Grid independence test and validation

Due to the V-shaped absorber plate inside the computational plane, the structural mapped grids with orthogonal elements could not be applied. So, the domain of solution was discretized using unstructured triangular grids with clustering near the boundaries. To get the optimum number of elements, grid independence test was performed. In the mesh study, five different grid sizes with 21498 to 82590 elements were examined, and the maximum absorber temperature as the parameter most sensitive to the grid size was evaluated and reported in Table 2. The discretized computational domain with 58993 elements is best suited for this model beyond this mesh size, and the percentage of maximum temperature variation becomes less than 1%. In Fig. 3, the discretized computational domains in some parts of solar collector are depicted.

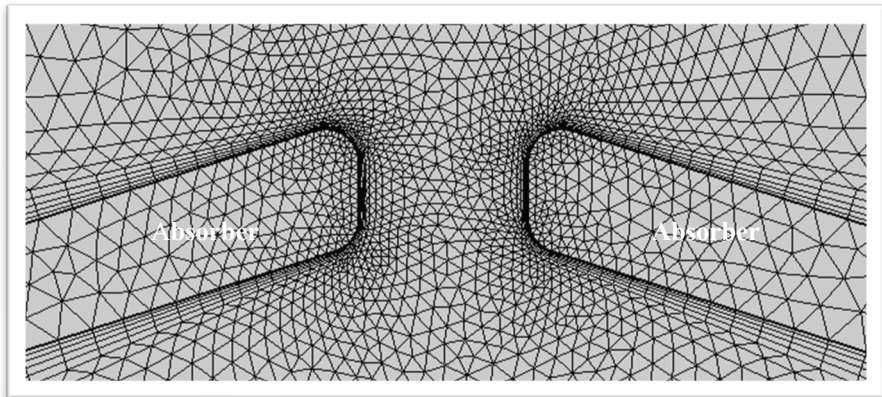
No. of elements	T_{max}	Variation respect to previous step
21498	366.8	-
30098	352.2	3.9%
42137	345.6	1.9%
58993	342.2	1%
82590	340.9	0.4%

Table 2. Mesh study.

In the present simulation, the wall function is used for flow simulation adjacent to the solid walls and the minimum size of elements in the computational domain is chosen based on $y^+ \geq 30$ as computed by Bejan (2013).



(a)



(b)

Fig. 3. Schematic of the discretized computational domain. (a) Grids inside a portion of air duct including the V-shaped absorber; (b) Zoomed image near the grooved absorber.

The applied physical model and numerical simulation were validated with the experimental data by Chabane (2014). The plane SAH, which was studied experimentally in that study, is analyzed here and the numerical results are compared with the experimental data. The efficiency of SAH is evaluated at two different air mass flow rates and its distributions from 9 a.m. to 14 p.m. are plotted in Fig. 4. This figure shows higher thermal efficiency as the mass flow rate gets higher values, such that the maximum efficiency occurs at 1 p.m., while the incoming solar radiation has its maximum value. The maximum difference between the predicted thermal efficiency and experimental data with the percentage of 5.5% takes place for the air mass flow rate $\dot{m} = 0.01 \text{ kg/s}$, at 11 a.m., which shows the acceptable accuracy of computations.

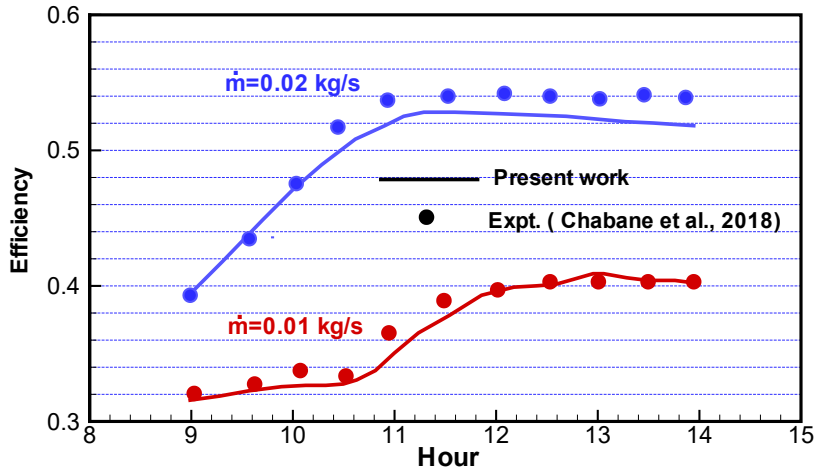


Fig. 4. SAH efficiency at different hours, comparison with experimental data Chabane (2014).

4. Results

The flow and thermal behavior of SAHs with a new type of V-corrugated absorber plate are examined in this paper. The use of suggested absorber has three benefits including the increasing surface of heat transfer, prevention of separation due to suction and the jet impingement technique, simultaneously. In several test cases analyzed in this paper, the performance of SAH was verified at different air mass flow rate, sun heat flux and the height of V-shaped absorber plate. In Fig. 5, the contours of velocity magnitude in upper and lower air ducts of heater are plotted. It should be noted that for having the same rate of suction process via the eight grooves, the variable groove thickness t is considered, such that the first groove at the upstream side has the maximum thickness $t_0 = 4 \text{ mm}$, and this value decrease for the next grooves by 20%. Figure 5 shows high velocity regions on the top edges of absorber plate where the suction process not only maintains the convection flow adjacent to the absorber surface, but also produces air jets toward the heated bottom plate. The zoomed image depicted in Fig. 5 shows these positive influences of the installed grooves on the absorber plate. The flow pattern inside the solar collector can also be shown by plotting the streamline in Fig. 6. The impact of grooves and suction process through these elements are easily seen in this figure.

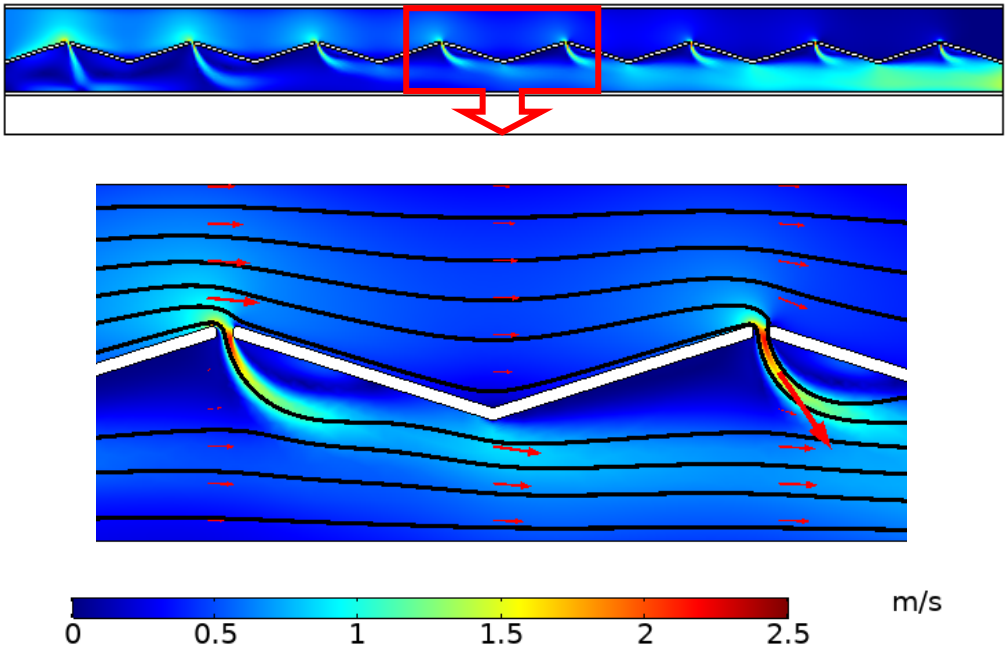


Fig. 5. Velocity magnitude contour and steam line plot, $q_{sun} = 1100W / m^2$.

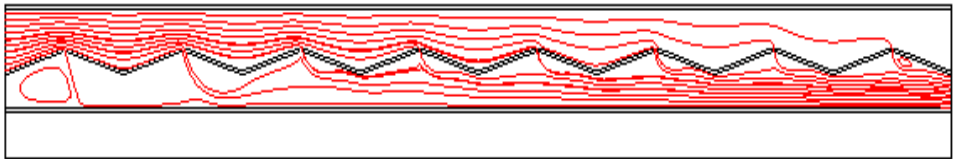


Fig. 6. Stream line plot.

The pressure contour drawn in Fig. 7 shows a relatively high-pressure zone with almost uniform distribution inside the upper duct and low pressure in the lower duct, where the air pressure decreases along the flow direction. The computed air pressure reveals the pressure drop of $\Delta p = 3 Pa$ through the heater.

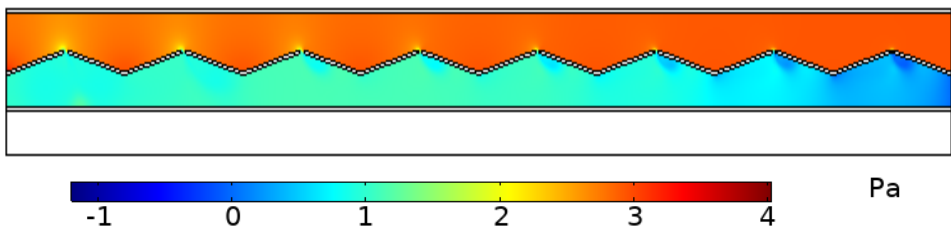


Fig. 7. Pressure contours, $q_{sun} = 1100W / m^2$.

The contour plot of turbulent kinetic energy is depicted in Fig. 8. This figure shows high turbulent kinetic energy inside the air jets, especially closed to the outlet flow from the grooves.

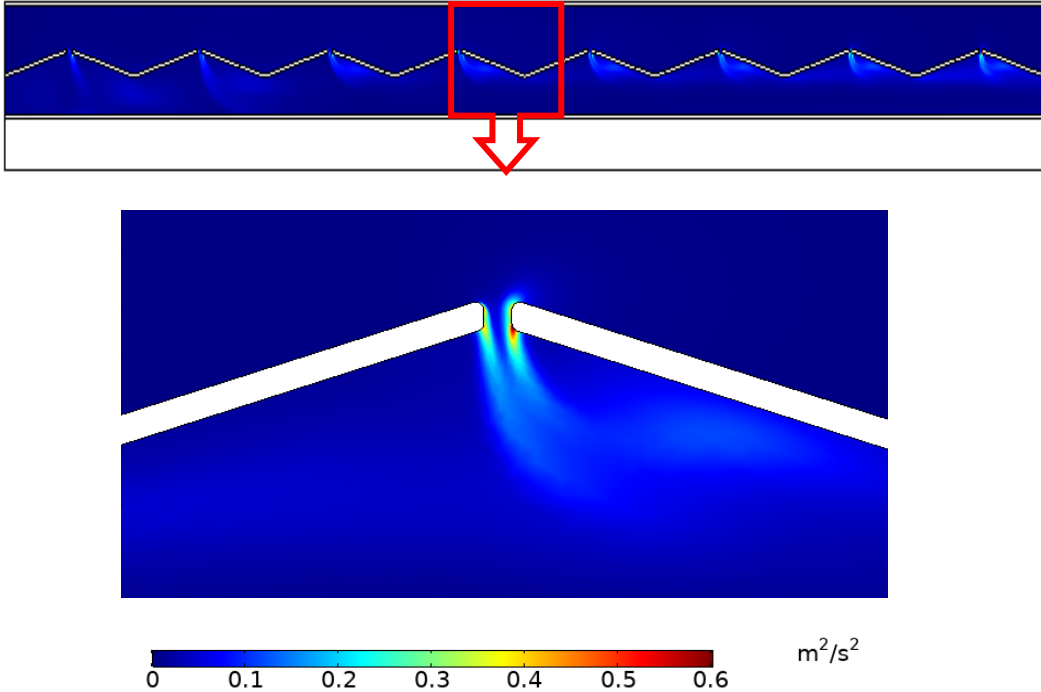


Fig. 8. Contours of turbulent kinetic energy, $q_{sun} = 1100W / m^2$.

To demonstrate the thermal behavior of solar collector, the temperature contour plots inside the whole parts of SAH at three different solar irradiations are depicted in Fig. 9. The highest temperature belongs to the absorber where the incoming solar irradiation is absorber. Also, due to the surface radiation, the bottom plate and glass cover have relatively high temperatures and some of the energy conversion between solar radiation into air enthalpy takes place by convection with these elements. The comparison between the contour plots in Fig. 9 demonstrates the temperature increase in the whole parts of SAH as the incoming solar heat flux gets higher values. Because of the effective applied technique in the proposed SAH and high performance of the heater in converting radiative energy into gas enthalpy, the absorber temperature is not too high, such that the maximum absorber temperature that occurs in the case of $q_{sun} = 1100 W/m^2$, is about 343 K. If one compares the air temperature inside the upper and lower ducts, it can be found that the suction process by the installed grooves on the absorber has the main role in increasing the air temperature, such that the fluid temperature inside the lower duct is much higher than in the upper channel.

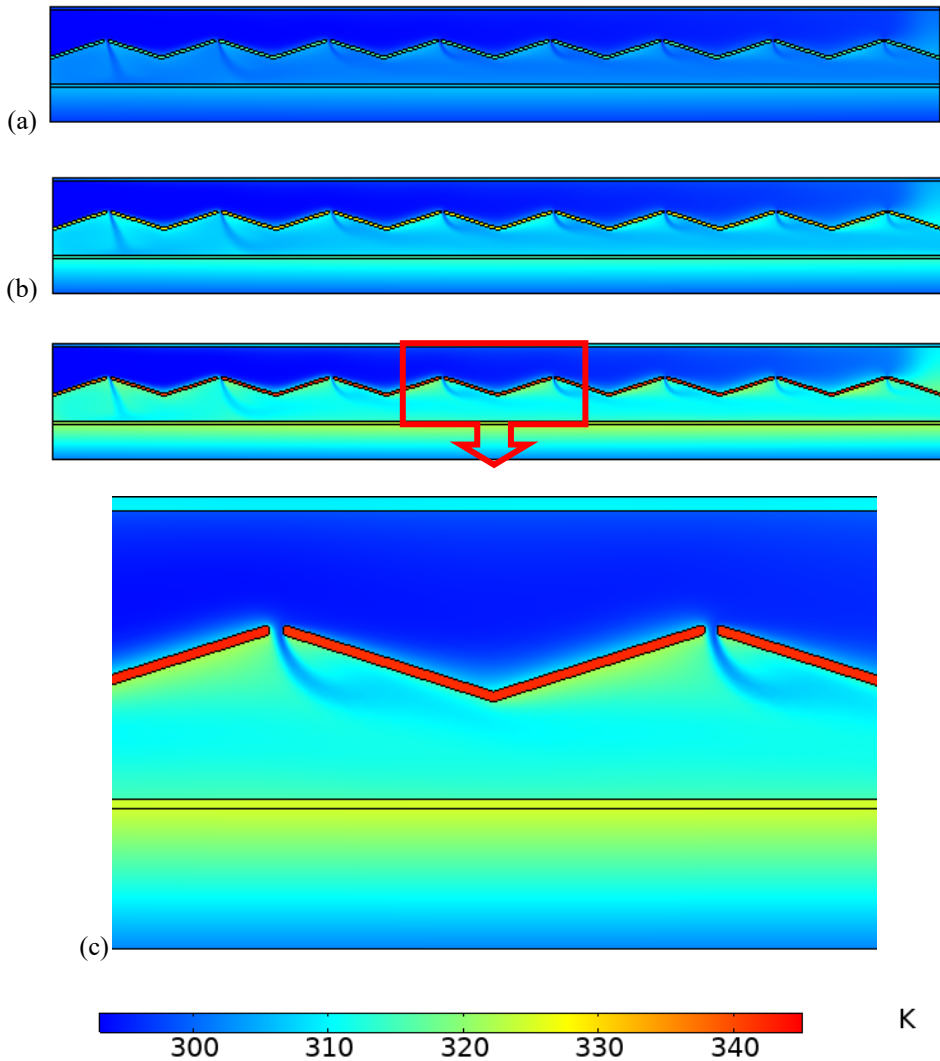


Fig. 9. Temperature contours at different Sun heat flux.

To show the positive impact of the proposed absorber plate in increasing the air temperature, the distributions of air bulk temperature along the two ducts of heater are drawn in Fig. 10. As seen before in the previous figures, the air temperature inside the lower duct is much higher than the upper air channel. For explanation of Fig. 10, it is worth mentioning that because of the air suction through the installed grooves on the absorber plate, the air mass flow rate inside the upper duct decreases along the flow direction and the opposite manner exists in the lower duct. Because of this fact, an almost uniform air temperature along the x-direction takes place in the lower duct. The sudden temperature drops at the upstream side in this air duct is due to the mixing process and injection of cold air into the high temperature air flow in the lower channel. The high rate of temperature increase in the air flow near the suction $x=L$ inside the upper air duct is due to the decrease in the air mass flow rate and heat capacity along the flow direction. Figure 10 also shows the impact of solar irradiation on the air temperature rise. As seen, the air temperature increases

with the increase in solar heat flux especially in the lower duct and higher outlet air temperature takes place in the heater as the solar irradiation gets higher values.

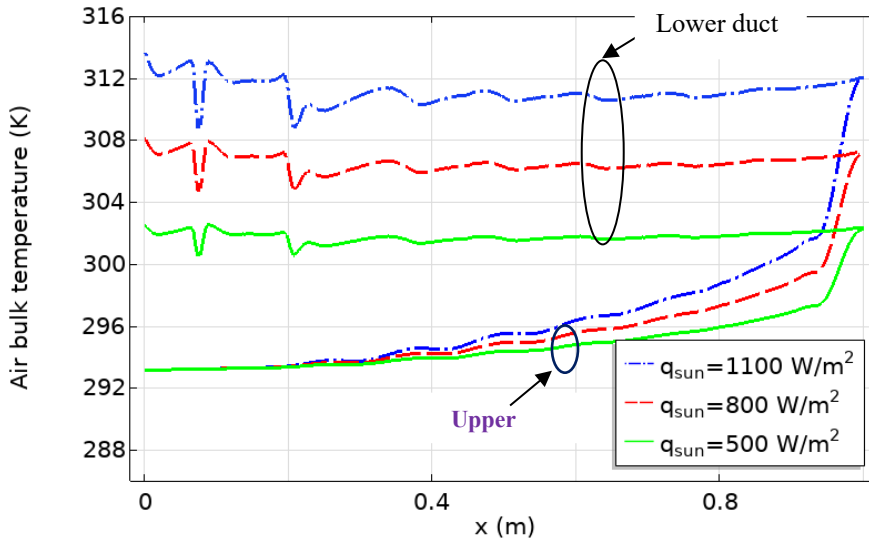


Fig. 10. Air bulk temperature distributions along the upper and lower ducts.

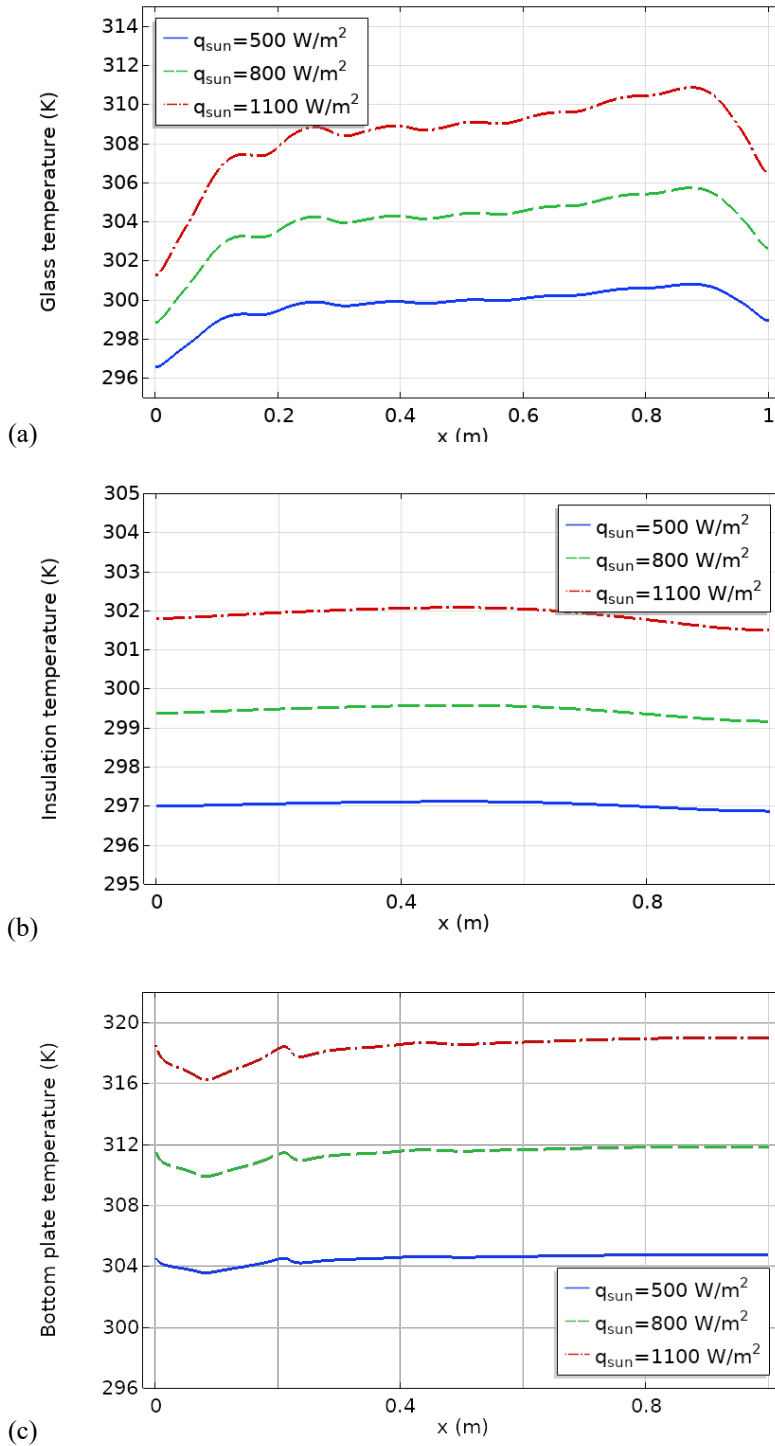


Fig. 11. Temperature distributions along (a) glass cover; (b) insulation; (c) bottom plate at different solar incoming radiation.

The temperature distributions along the axial direction on the external surfaces of glass cover and insulation layer and on the upper surface of the bottom plate are plotted in Fig. 11. It can be seen that these temperatures have increasing trends by increase in the incoming solar radiation. For the glass cover, the minimum temperatures occur at the two ends and the glass temperature is relatively high in the vicinity of the central region. Also, almost uniform temperatures take place on the surfaces of the insulation layer and bottom plate. For the purpose of demonstrating the absorber temperature, the temperature contours inside this element are drawn in Fig. 12 for $q_{sun} = 1100 \text{ W/m}^2$. It can be noticed that the absorber temperature, which is in the range of $335.2 \text{ K} \leq T \leq 342.4 \text{ K}$, varies along the flow direction with both increasing and decreasing local trends such that the maximum temperature occurs near the section $x=7L/8$ and the minimum temperature at $x=0$. It should be recalled that, as reported for the simple plane SAHs with a smooth rectangular absorber plate in literature, the absorber temperature increases along the flow direction due to the growth of thermal boundary layer (Bejan (2013)); however, due to the suction and mixing processes inside the heater with the proposed absorber, the absorber temperature varies with fluctuations, as shown in Fig. 12.

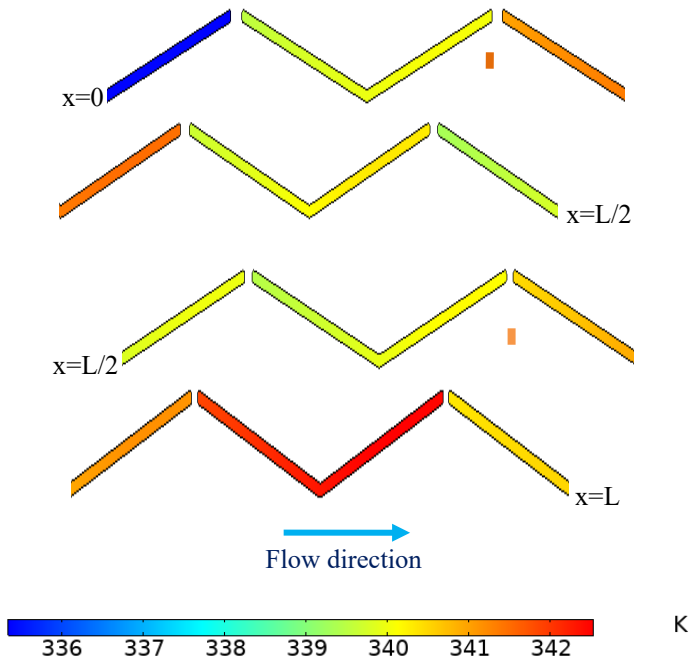


Fig. 12. Temperature field inside the V- corrugated absorber, $q_{sun} = 1100 \text{ W / m}^2$.

It is clear that the height of V-shaped absorber i.e. H_0 as the main geometrical parameter has a great effect on the performance of the heater. To examine the effect of this parameter, the contours of velocity magnitude and temperature are drawn in Figs. 13 and 14 at three different values of the H_0 . As this parameter increases, Fig. 13 shows higher rate of suction process that enhances the jet impingement effect, such that the jet flows are more inclined to the downstream side. On the other hand, it is clear that the air velocity and the blockage effect in the upper duct increases as H_0 gets higher value and more pressure drop takes place inside the SAH. Figure 14 shows that H_0 has a great impact on the temperature field inside the SAH such that higher air

temperature with more uniformity is seen inside the lower duct which is due to stronger jet impingement effect and mixing processes for the large value of the parameter H_0 .

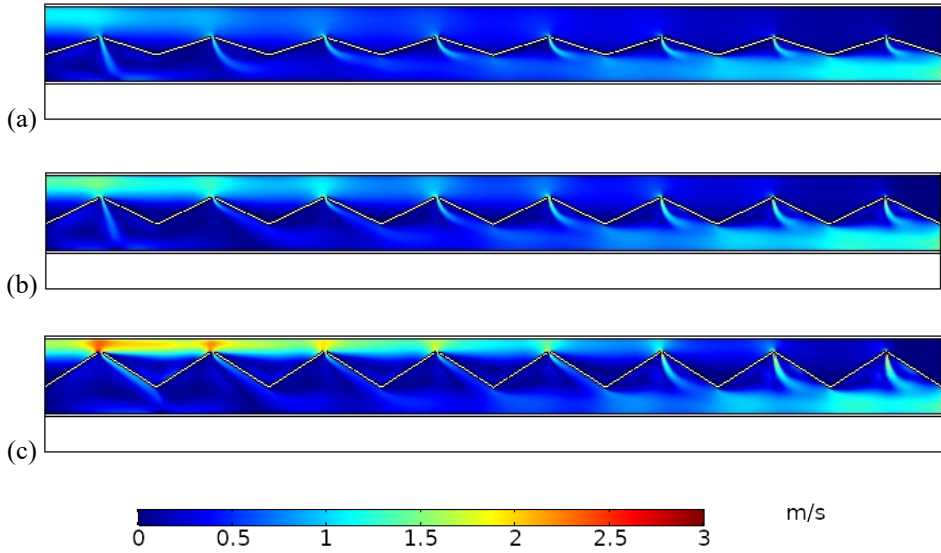


Fig. 13. Velocity magnitude contours at different values of the parameter H_0 , (a) $H_0=2\text{cm}$; (b) $H_0=3\text{cm}$; (c) $H_0=4\text{cm}$.

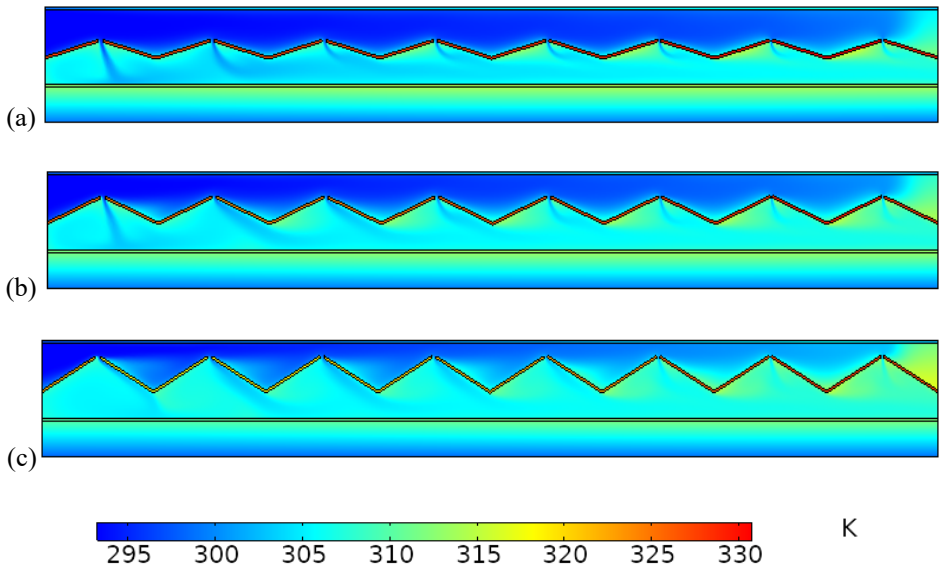
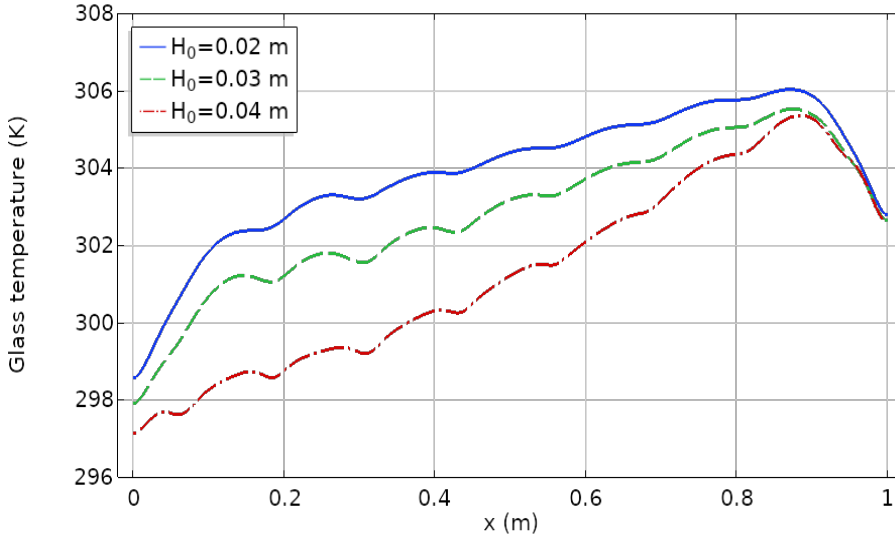
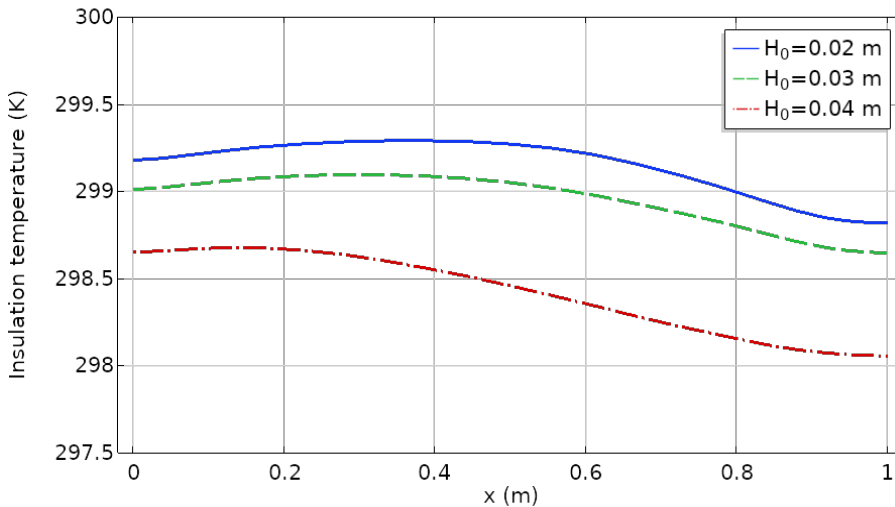


Fig. 14. Temperature contours at different values of the parameter H_0 , (a) $H_0=2\text{cm}$; (b) $H_0=3\text{cm}$; (c) $H_0=4\text{cm}$.

To analyze the effect of absorber height H_0 on the thermal behavior of SAH, the temperature distributions along the external surfaces of solar collector, i.e. glass cover and insulation, are drawn in Fig. 15. As can be seen, the temperature decrease happens on the surfaces of these boundaries as the parameter H_0 gets higher values. So, it is expected that the rates of heat transfer from these surfaces to the surrounding, which are the two main sources of heat loss in the solar collector, will decrease and the SAH will have higher performance.



(a) glass temperature distribution



(b) Insulation temperature distribution

Fig. 15. Temperature distributions along the (a) glass cover; (b) insulation layer at different values of parameter H_0 , $\dot{m} = 0.04 \text{ kg / s}$, $q_{sun} = 800 \text{ W / m}^2$.

Entropy generation

From the second law point of view, the performance of the proposed SAH is also studied here. For this purpose, the entropy generation inside the solar collector which is due to both friction and heat transfer is computed from the obtained velocity and temperature fields. The rate of entropy generation per unit time and per unit volume as given by Bejan (2013) is as follows:

$$\dot{s}_{gen} = \frac{k}{T^2} \left[\left(\frac{\partial T}{\partial x} \right)^2 + \left(\frac{\partial T}{\partial y} \right)^2 \right] + \frac{\mu}{T} \left\{ 2 \left[\left(\frac{\partial u}{\partial x} \right)^2 + \left(\frac{\partial v}{\partial y} \right)^2 \right] + \left(\frac{\partial u}{\partial y} + \frac{\partial v}{\partial x} \right)^2 \right\} \quad (9)$$

Where the first term in the RHS is the entropy generation due to viscous friction and the second term is the entropy generation because of the heat transfer. Also, the total entropy generation that shows the amount of irreversibilities due to both viscous friction and heat transfer can be expressed as:

$$\dot{S}_{gen} = \int_{\forall} \dot{s}_{gen} d\forall \quad (10)$$

where \forall is the volume of flow domain. The contours of entropy generation inside the air flow at three different solar heat fluxes are drawn in Fig. 16. This figure reveals a high rate of irreversibility near the absorber plate due to high temperature and velocity gradients in this region. Also, a high rate of entropy generation is seen inside the air jets from the grooves. In the region far from the absorber, a low rate of entropy generation that shows more reversible process takes place. Besides, the comparison between the contour plots in Fig. 16 reveals higher rate of irreversibilities with an increase in the value of the solar heat flux. (a)

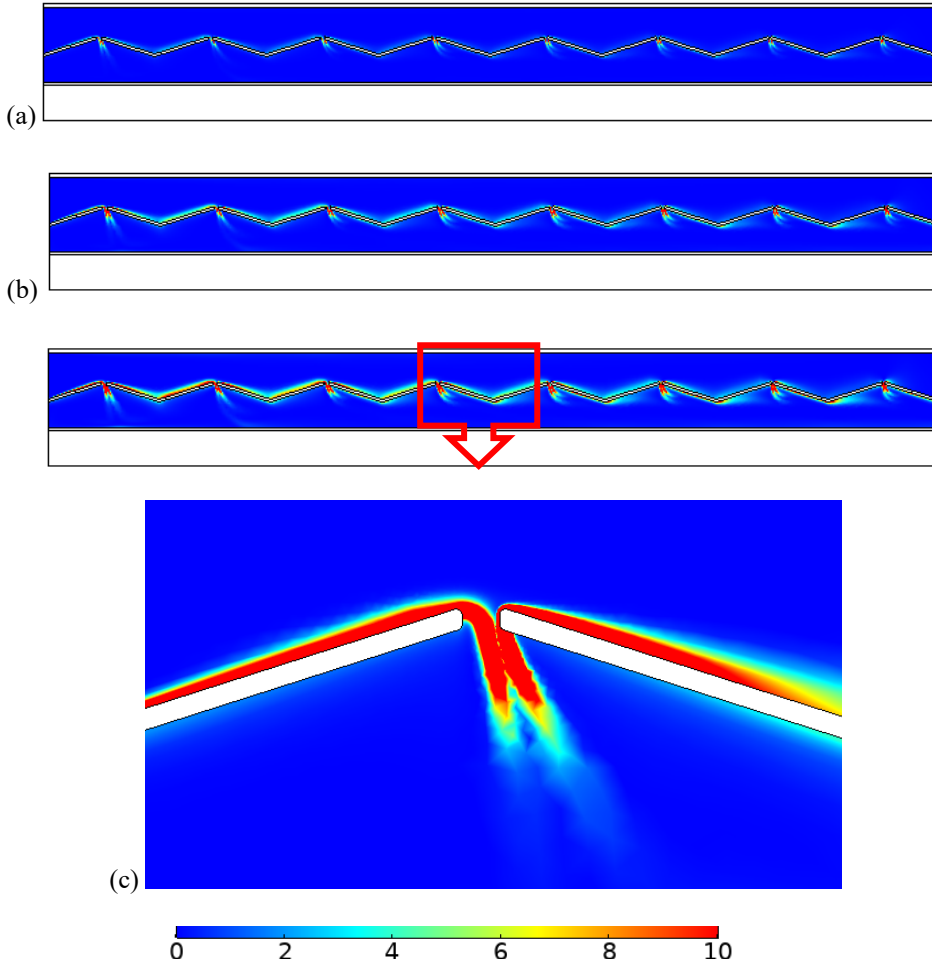


Fig. 16. Contours of entropy generation inside the air flow; (a) $q_{sun} = 500 \text{ W} / \text{m}^2$; (b) $q_{sun} = 800 \text{ W} / \text{m}^2$; (C) $q_{sun} = 1100 \text{ W} / \text{m}^2$.

The entropy generation inside the solid elements due to conduction heat transfer is studied in Fig. 17 by plotting the contour of this parameter at three different values of the solar heat flux. The comparison between the contour plots shows higher rate of irreversibility as the incoming radiation gets higher values. The entropy generation inside the insulation layer and glass cover has a relatively uniform distribution but for the absorber plate where very high temperature gradient in the axial direction takes place due to air suction by the grooves and the existence of flow vortices, the entropy generation varies considerably. Also, if one compares Figs. 16 and 17 with each other, it can be revealed that most of the entropy generation inside the solar collector is due to the viscous friction.

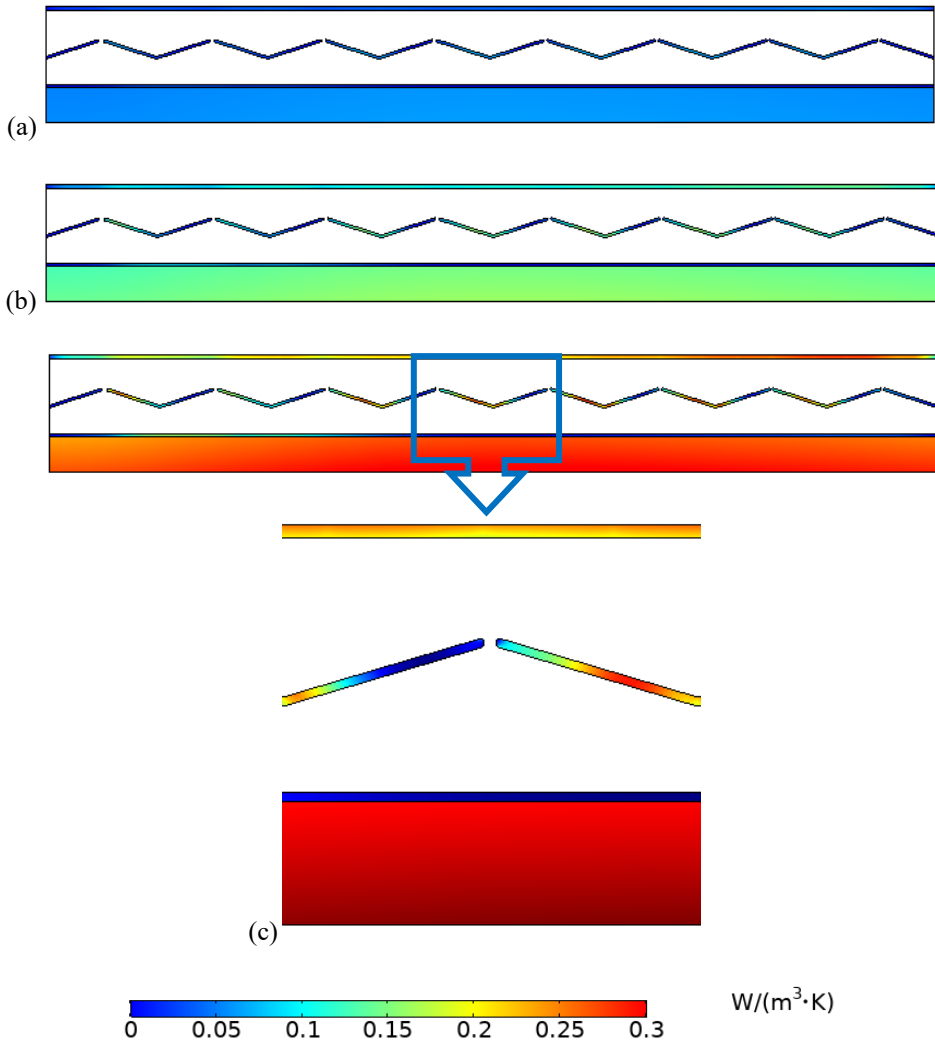


Fig. 17. Contours of entropy generation inside the solid elements. (a) $q_{sun} = 500 \text{ W} / \text{m}^2$; (b) $q_{sun} = 800 \text{ W} / \text{m}^2$; (C) $q_{sun} = 1100 \text{ W} / \text{m}^2$.

4.2 The first and second law efficiencies

The thermal efficiency (first law efficiency) of SAH is one of the main parameters that shows the performance of the solar collector in converting thermal radiation into gas enthalpy. To demonstrate the performance of the proposed SAH, the thermal efficiency at different steady conditions is calculated according to the following relation:

$$\eta_I = \frac{\dot{m}c_p(T_{mout} - T_{in})}{q_{sun} \cdot A} \quad (11)$$

In Fig. 18, the distributions of collector efficiency with solar heat flux at different values of the air mass flow rates are plotted. Moreover, a comparison is made between the efficiency of the proposed SAH and its competitor with a simple V-corrugated absorber plate shown in Fig. 19. As seen, the proposed SAH has relatively high thermal efficiency, especially when the solar collector operates at large value of air mass flow rate and low incoming solar heat flux, such that up to 80% for the value of thermal efficiency is predicted. If one compares the collector efficiency of the suggested SAH with its competitor shown in Fig. 19, up to 10% increase in the value of thermal efficiency can be calculated. Although the SAH shown in Fig. 19 is a double pass type, higher efficiency for the proposed SAH reveals the positive impact of the grooved V-corrugated absorber plate in convection enhancement between the heated surface and turbulent air flow.

It is expected that the thermal efficiency under the optimum design can get even higher values. For this, the variations of solar heater efficiency against the air mass flow rate at three different values of the geometrical parameter H_0 are drawn in Fig. 20. This figure shows that under the optimum value of $H_0 = 4 \text{ cm}$, the solar collector has the maximum efficiency, such that the computations showed that for $H_0 > 4 \text{ cm}$, the opposite trend for the thermal efficiency takes place.

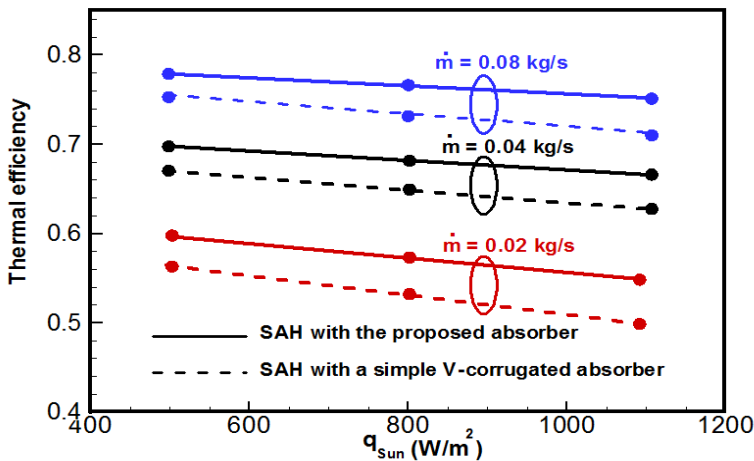


Fig. 18. Variation of thermal efficiency with sun heat flux, $H_0 = 2 \text{ cm}$.

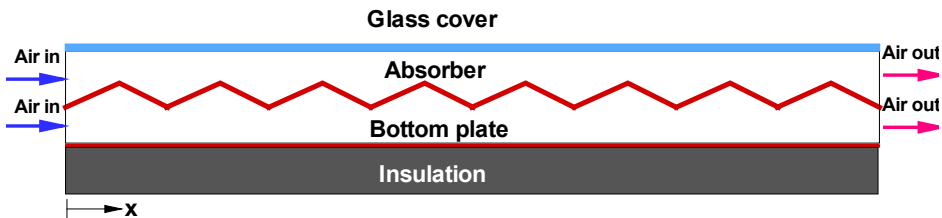


Fig. 19. The schematic of the SAH with a simple V-corrugated absorber.

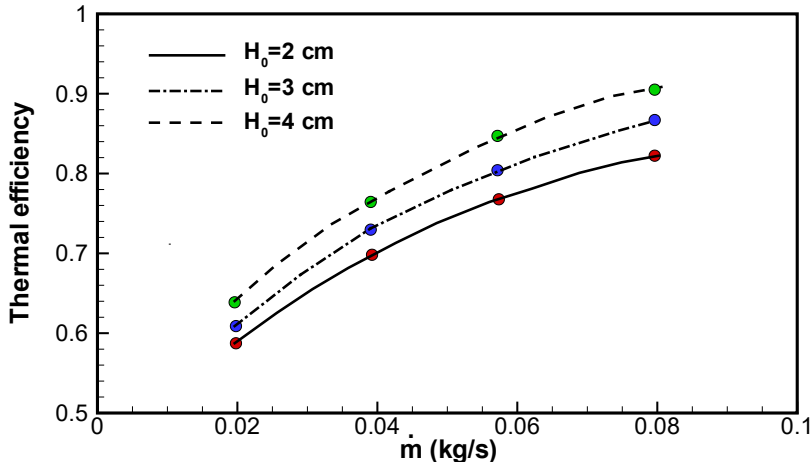


Fig. 20. The distribution of collector efficiency with air mass flow rate, $q_{sun} = 800 \text{ W} / \text{m}^2$.

Finally, to evaluate the amount of irreversibilities in the studied thermal system, the second law efficiency is computed. The exergy efficiency of SAH was evaluated using the following equation as Hassan (2022):

$$\eta_2 = 1 - \left(\frac{\dot{E}_{xdes}}{\left(1 - \left(\frac{T_{amb}}{T_s}\right)\right)\dot{Q}_s} \right) \quad (12)$$

Where the distractive exergy, \dot{E}_{xdes} , is computed based on the following relation:

$$\Sigma \left(1 - \frac{T_{amb}}{T_{sun}} \right) \dot{Q}_{sun} - \dot{m}(h_{out} - h_{in}) - T_{amb}(s_{out} - s_{in}) \quad (13)$$

The variations of the second law efficiency with the incoming solar heat flux are drawn in Fig. 21. As can be seen, the second law efficiency has small value due to the high temperature of the heat source (Sun), such that the value of this parameter increases with the increase in solar heat flux and decrease in air mass flow rate.

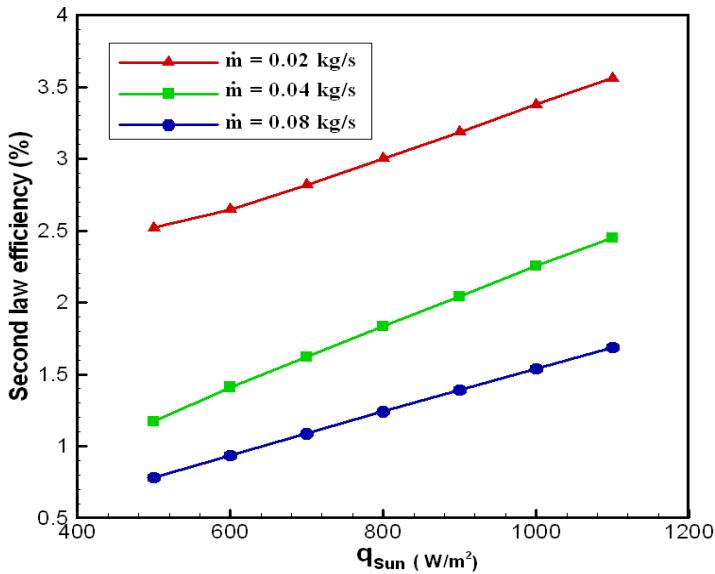


Fig. 21. The variation of second law efficiency with solar heat flux at different air mass flow rates.

5. Conclusion

One of the best forms of renewable energy is solar energy and SAHs which usually have simple configurations are useful heat exchangers for converting solar irradiation into air enthalpy. In this article, we performed a CFD- based numerical analysis to examine the benefits of using a new type of V-corrugated absorber plate for higher performance. It is claimed that the proposed absorber fulfills the three efficient techniques for improving the performance of SAHs, simultaneously. These techniques are the extension of the heat transfer surface area, suction process for keeping the convective flow closed to the heated absorber surface and jet impingement method. The present numerical analysis involves the solution of flow equations with the finite element scheme by the COMSOL Multi-physics. Numerical findings demonstrate about 10% improvement in the thermal efficiency of the proposed solar collector compared with its competitor (SAH with a simple V-corrugated absorber) under the same operating conditions. Also, the effect of V-shape absorber's height on the heater performance is studied and the increasing in the value of this parameter from $H_0 = 2 \text{ cm}$ to $H_0 = 4 \text{ cm}$ leads to about 11% improvement in thermal efficiency. Finally, the entropy generation study reveals the dominance of viscous friction compared with the heat transfer in the formation of irreversibilities in solar collector. As the next step in designing more efficient SAHs, the authors are going to study the combination of the present configuration with other existing techniques, such as using fins and vortex generators for having the maximum possible SAH performance.

Nomenclature

A	Area (m ²)	ρ_g	Glass reflectivity
b	Height of channel (m)	τ_g	Glass transmissivity
C_p	Specific heat (kJ/kg K)	μ	Fluid Viscosity (Pa.s)
D_h	Hydraulic diameter (m)	ρ	Fluid density (kg/m ³)
$\dot{E}_{x_{des}}$	Distractive exergy (W/m ²)	κ	Turbulence kinetic energy (m ² /s ²)
h	Convection coefficient (W/m ² K)	ε	Surface emissivity
$h_{in,out}$	Inlet(outlet) air enthalpy(kJ/kg)	ε	Turbulent dissipation rate (m ² /s ²)
H_0	Geometrical parameter (m)	δ	Thickness (m)
k	Thermal conductivity (Wm ⁻¹ K ⁻¹)	Subscript	
L	Length of heater (m)	abs	Absorber
L_0	Geometrical parameter (m)	amb	Ambient
p	Pressure (Pa)	conv	Convection
Pr	Prandtl number	g	Glass
q	Heat flux (W/m ²)	gen	Generation
Re	Reynolds number	in	Inlet
s	Entropy (kJ/kg K)	ins	Insulation
T	Temperature (K)	i, j	Tensor indices
t_0	The maximum groove thickness (m)	m	Mean
V	Velocity vector (m/s)	out	Outlet
(x, y)	Coordinates (m)	rad	Radiation
y_0	Geometrical parameter (m)	t	Turbulent
Greek symbols		bp	Bottom plate
α_g	Glass absorptivity	s	Sun

References

- Afshari F, Sözen A, Khanlari A, Tuncer A.D and Şirin C (2020). Effect of turbulator modifications on the thermal performance of cost-effective alternative solar air heater, *Renewable Energy*, 158, 297-310.
- Agrawal Y, Bhagoria J and Pagey V.S (2022). Enhancement of thermal efficiency of solar air collector by using discrete double arc reverse shaped roughness on the absorber plate, *Materials Today: Proceedings*, 51, 1548-1553.
- Alam T and Kim M.H (2017). Heat transfer enhancement in solar air heater duct with conical protrusion roughness ribs, *Applied Thermal Engineering*, 126, 458-469.
- Alomar O.R, Abd H.M and Salih M.M.M (2022). Efficiency enhancement of solar air heater collector by modifying jet impingement with v-corrugated absorber plate, *Journal of Energy Storage*, 55 (2022) 105535.

- Arya N, Goel V and Sunden B (2023). Solar air heater performance enhancement with differently shaped miniature combined with dimple shaped roughness: CFD and experimental analysis, *Solar Energy*, 250, 33-50.
- Bayrak F, Oztop H.F and Hepbasli A (2013). Energy and exergy analyses of porous baffles inserted solar air heaters for building applications, *Energy and Buildings*, 57, 338-345.
- Bejan A, (2013). *Convection heat transfer*, John Wiley & sons.
- Chabane F, Moumimi N and Benramache S (2014). Experimental study of heat transfer and thermal performance with longitudinal fins of solar air heater, *Journal of advanced research*, 5(2), 183-192.
- Desisa D.G and Shekata G.D (2020). Performance Analysis of Flat-Plate and V-groove Solar Air Heater Through CFD Simulation, *International Journal of Renewable Energy Development*, 9(3),369-381.
- Duffie J.A and Beckman W.A, (2013). *Solar engineering of thermal processes*, John Wiley & Sons.
- El-Said E.M (2020). Numerical investigations of fluid flow and heat transfer characteristics in solar air collector with curved perforated baffles, *Engineering Reports*, 2(4), e12142.
- El-Sebaïi A, Aboul-Enein S, Ramadan M, Shalaby S, Moharram B (2011). Investigation of thermal performance of-double pass-flat and v-corrugated plate solar air heaters, *Energy*, 36(2), 1076-1086.
- Fiuk J.J and Dutkowski K (2019). Experimental investigations on thermal efficiency of a prototype passive solar air collector with wavelike baffles, *Solar Energy*, 188, 495-506.
- Hachemi A (1995). Thermal performance enhancement of solar air heaters, by a fan-blown absorber plate with rectangular fins, *International journal of energy research*, 19(7), 567-577.
- Hassan A, Nikbahkt A.M, Welsh Z, Yarlagadda P and Fawzia S, Karim A (2022). Experimental and thermodynamic analysis of solar air dryer equipped with V-groove double pass collector: Techno-economic and exergetic measures, *Energy Conversion and Management: X*, 16, 100296.
- Ho C.-D, Hsiao C.-F, Chang H, Tien Y.-E and Hong Z.-S (2017). Efficiency of recycling double-pass V-corrugated solar air collectors, *Energies*, 10(7), 875.
- Khanlari A, Sözen A, Afshari F, Tuncer A.D, Ağbulut Ü and Yılmaz Z.A (2021). Numerical and experimental analysis of parallel-pass forced convection solar air heating wall with different plenum and absorber configurations, *International Journal of Numerical Methods for Heat & Fluid Flow*, 978-1001.
- Mohammadi K and Sabzpooshani M (2013). Comprehensive performance evaluation and parametric studies of single pass solar air heater with fins and baffles attached over the absorber plate, *Energy*, 57, 741-750.
- Nidhul K, Yadav A.K and Anish S, Arunachala U (2020). Efficient design of an artificially roughened solar air heater with semi-cylindrical side walls: CFD and exergy analysis, *Solar Energy*, 207, 289-304.
- Patankar S (1966). Heat transfer across a turbulent boundary layer: Application of a profile method to the step-wall-temperature problem, *International Journal of Heat and Mass Transfer*, 9(8), 829-834.
- Saravanakumar P, Somasundaram D, Matheswaran M (2020). Exergetic investigation and optimization of arc shaped rib roughened solar air heater integrated with fins and baffles, *Applied Thermal Engineering*, 175, 115316.
- Wang D, Liu J, Liu Y, Wang Y, Li B and Liu J (2020). Evaluation of the performance of an improved solar air heater with “S” shaped ribs with gap, *Solar Energy*, 195, 89-101.
- Yang M, Yang X, Li X, Wang Z and Wang P (2014). Design and optimization of a solar air heater with offset strip fin absorber plate, *Applied Energy*, 113, 1349-1362.